

Nominal doping and partition of doped holes between planar and apical orbitals in $\text{La}_{2-x}\text{Sr}_x\text{CuO}_4$

E. S. Božin and S. J. L. Billinge

*Department of Physics and Astronomy, Michigan State University, East Lansing, MI 48824**

(Dated: November 4, 2018)

By considering both the average structural parameters obtained from Rietveld refinement of neutron powder diffraction data, and the local structural parameters obtained from the atomic pair distribution function, we have tested the recent hypothesis of Perry *et al.* [Perry *et al.*, Phys. Rev. B **65**, 144501 (2002)] that doping in $\text{La}_{2-x}\text{Sr}_x\text{CuO}_4$ system occurs as localized defects of predominantly $\text{Cu}d_{3z^2-r^2}-\text{O}p_z$ character associated with the Sr dopants accompanied by a local destruction of the Jahn-Teller distortion. While the structural parameters behave qualitatively according to the prediction of this model, a quantitative analysis indicates that doped holes predominantly appear in the planar $\text{Cu}d_{x^2-y^2}-\text{O}p_{x,y}$ band as is normally assumed. However, a small amount of the doped charge does enter the $\text{Cu}d_{3z^2-r^2}-\text{O}p_z$ orbitals and this should be taken into account when theoretical phase diagrams are compared to experiment. We present a calibration curve, $p = x(1.00(1) - 0.45(7)x)$, for the planar charge doping, p , vs strontium content, x , for the $\text{La}_{2-x}\text{Sr}_x\text{CuO}_4$ system.

PACS numbers: 74.81.-g, 74.72.Dn, 74.72.-h, 61.12.-q

I. INTRODUCTION

Cuprate high temperature superconductors are doped Mott insulators. The novel superconductivity appears at doping levels just beyond the insulator-metal (IM) transition. The insulating behavior of the undoped endmember is understood to be due to electron correlation effects in the half-filled planar $\text{Cu}d_{x^2-y^2}-\text{O}p_\alpha$ ($\alpha = x, y$) anti-bonding band. The phase diagram of the cuprates can be interpreted in terms of holes doped into this planar band. For example, in the system $\text{La}_{2-x}\text{Sr}_x\text{CuO}_4$ it is assumed that one hole enters this band per strontium atom. This paradigm for the doping has hardly been questioned and a multitude of papers exist implicitly assuming this behavior. The $\text{La}_{2-x}\text{Sr}_x\text{CuO}_4$ system is archetypal since it is a single layer system which can be straightforwardly doped over a wide range. The resulting phase diagram is thought to exhibit features that are universal to the cuprates. However, as a result of recent *ab initio* electronic band structure calculations, Perry, Tahir-Kheli and Goddard (PTG)¹ have suggested a new model for the doping in the $\text{La}_{2-x}\text{Sr}_x\text{CuO}_4$ system. In this case the doped holes reside in localized states on the CuO_6 octahedra situated next to the dopant strontium ions. Furthermore, the doped charge resides principally in the $\text{Cu}d_{3z^2-r^2}-\text{O}p_z$ orbitals (i.e., the out-of-plane bonds). Coincidentally a structural distortion occurs such that the local Jahn-Teller (JT) distortion, that results in the long Cu-O apical bond, is destroyed. A flat impurity band forms in the gap. The IM transition then occurs on increased doping in a manner similar to doped semiconductors by percolation of the doped impurities. These calculations were originally motivated by XAFS measurements that observed a distorted environment of the octahedra in the vicinity of dopant ions². This new way of understanding the doping, if it is right, clearly will result in a paradigm shift in our understanding of

cuprate physics. It is thus of the greatest importance to test the hypothesis experimentally. A rather direct probe of this doping mechanism is the structure because it involves the local destruction of JT elongated bonds. The *average* Cu-O bond length along z will thus shorten with doping and the width of the bond-length distribution for this bond will increase reflecting the increased disorder. Despite detailed structural studies of this system³ the temperature and doping dependence of these parameters has not been reported. In this paper we investigate whether there is evidence supporting this new doping paradigm in both the average crystal structure, and the local structure as measured using the atomic pair distribution function (PDF) technique⁴. We reexamine the extensive earlier structural data of Radaelli to extract the desired parameters. We have also analyzed new neutron powder diffraction data using Rietveld refinement and PDF refinement. We find that the data qualitatively agree with the predictions of the Perry *et al.*¹. However, a more quantitative analysis, including evaluating the bond valences as a function of doping of the in-plane and apical Cu-O bonds, indicates that doped charge is predominantly residing in the planar bonds suggesting the existing paradigm for doping is valid.

II. EXPERIMENTAL

This study reexamines the extensive published data of Radaelli *et al.*³ to extract as a function of doping the interesting parameters of the plane copper to apical oxygen bond length, $r_{\text{Cu}-\text{O}2}$ and the short lanthanum/strontium to apical oxygen bond length, $r_{\text{La/Sr}-\text{O}2}$. These parameters were determined from the reported fractional coordinates and lattice parameters. Also important is the doping dependence of the copper to in-plane oxygen bond length, $r_{\text{Cu}-\text{O}1}$, which was presented previously³ but is

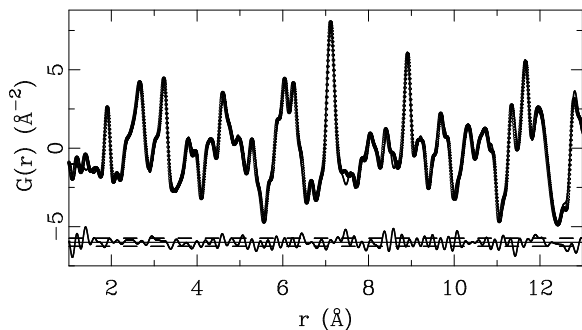


FIG. 1: Representative full profile PDF fit of standard LTO model to 10 K data for undoped sample. Experimental profile shown as open circles, model profile as solid line. Difference curve is shown below the fit as solid line. Dashed lines denote experimental uncertainties at the 2σ level. PDFs studied here utilize diffraction information up to $Q_{MAX} = 35 \text{ \AA}^{-1}$.

reexamined here. To check the PTG prediction we also need the anisotropic displacement parameter along the z -axis of the apical oxygen, $U_{33}(\text{O}2)$. This was not published in³ so we have used recently collected neutron powder diffraction data of our own from a less extensive set of samples. Samples were synthesized using solid state methods and loose powders of ~ 10 g sealed in vanadium cylinders were measured at 10 K at the GEM diffractometer at the ISIS neutron source. Details of sample synthesis, characterization and measurement are reported elsewhere^{5,6}. Rietveld refinements were carried out on the data using the program GSAS⁷. The data were also corrected for experimental effects and normalized to obtain the atomic pair distribution function⁸ (PDF) using the program PDFgetN⁹. The PDF is the Fourier transform of the normalized corrected powder diffraction data. It utilizes both Bragg and diffuse scattering and contains information about the local structure^{4,8}. Structural models were refined to the PDFs using the program PDFFIT¹⁰. To check for consistency, the same parameters were varied in the PDF and Rietveld refinements. An example of the measured PDF from the undoped sample is shown in Figure 1 with the best fit model-PDF plotted on top. The PDF allows us to explore models that contain non-periodic defects such as those proposed by PTG. The PDF was calculated from a supercell model with the doping induced defects discussed by PTG. This was then used as simulated data and fit using the usual long-range orthorhombic (LTO)³ structural model. In this way it was possible to estimate the size of the enlarged displacement factors that would result from the presence of the doping induced disorder described by PTG. In Perry *et al.*¹, for simplicity, no octahedral tilts were considered. In the present case we must compare resulting models with real data and so the doping induced defects described in¹ were superimposed on the background of octahedral tilts observed in the undoped endmember.

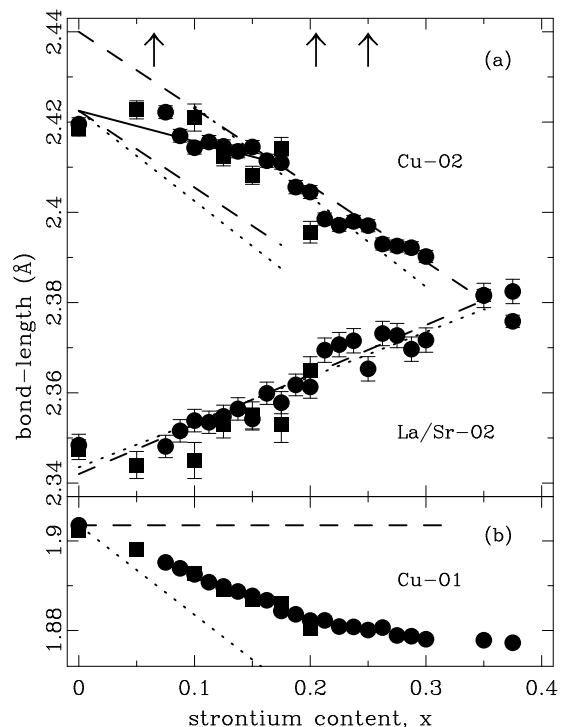


FIG. 2: Evolution of $r_{\text{Cu-O}2}$ and $r_{\text{La/Sr-O}2}$ (a), and $r_{\text{Cu-O}1}$ (b) average bond lengths with hole doping at 10 K: Rietveld result from³ (solid circles) and PDF result (solid squares). Dotted lines: slope predicted from simple electrostatics considerations. Dashed lines: slope prediction based on PTG model. Arrows (from left to right): IM transition, structural phase transition, and disappearance of superconductivity.

III. RESULTS AND DISCUSSION

The qualitative predictions for the evolution of the average structure with doping in the scenario of Perry *et al.*¹ are: (1) decrease in the average $r_{\text{Cu-O}2}$ due to the local destruction of Jahn-Teller distortions at Cu^{3+} sites; (2) increase in the $U_{33}(\text{O}2)$ with doping because of the coexistence of Jahn-Teller distorted and non-Jahn-Teller distorted octahedra; (3) increase in the average $r_{\text{La/Sr-O}2}$ distance. All these effects are seen qualitatively in the data as shown in Figs. 2 and 3.

However, similar effects can be expected even if the doping is taking place in the conventional way: homogeneously into the planar bonds. For example, if the CuO_2 planes are becoming more positively charged with doping the negatively charged apical oxygen would be predicted to come closer to the planes due to simple coulomb attraction. Also, the U_{33} displacement factor of the apical oxygen atom is expected to increase with doping due to the random doping of larger Sr^{2+} ions. Inhomogeneous doping in the form of stripes or checkerboards^{11,12} would also result in enlarged thermal factors for in-plane and apical motions of $\text{O}1$ and $\text{O}2$. However, inhomogeneous doping would not affect average bond-length obtained

from Rietveld refinement. It is therefore important to be more quantitative to distinguish these different possibilities.

The PTG calculations¹ were carried out at special rational doping fractions of 1/8, 1/4 and 1/2 and suggest the appearance of a single distorted CuO_6 octahedron associated with each doped strontium. The $r_{\text{Cu-O}2}$ bond closest to the strontium is shortened by $\Delta r_{\text{Cu-O}2} = -0.24 \text{ \AA}$ and that farthest from the Sr on the same octahedron by $\Delta r_{\text{Cu-O}2} = -0.10 \text{ \AA}$, the Sr-O2 distance increases, $\Delta r_{\text{La/Sr-O}2} = +0.11 \text{ \AA}$ and the in-plane $r_{\text{Cu-O}1}$ distances do not change. In the average structure these defects are not seen explicitly; however, the distortions will be apparent as a properly weighted change in the average bond-length and an increase in the respective displacement parameters. If we assume that these defects appear as each strontium is doped and are not a special feature of the rational doping fractions studied, we get the following relations for the strontium doping, x , dependence of the average bond lengths:

$$\Delta r_{\text{Cu-O}2}(x) = -0.17 x, \quad \Delta r_{\text{La/Sr-O}2}(x) = 0.11 x, \quad (1)$$

where x is the doping level. These are shown as the dashed lines in Fig. 2. The evolution of $r_{\text{La/Sr-O}2}$ is in quantitative agreement. The case of $r_{\text{Cu-O}2}$ is more complicated. $r_{\text{Cu-O}2}$ decreases much more slowly than the prediction initially on doping. However, beyond a doping level of ~ 0.17 the slope of $r_{\text{Cu-O}2}$ vs x increases. In this higher doping region the slope of the PTG line agrees rather well with the data. There is no specific prediction from the PTG calculations for the x -dependence of $r_{\text{Cu-O}1}$, although it is expected to be small since the length of $r_{\text{Cu-O}1}$ in the defect octahedra does not change and no doping dependent change in lattice parameters has been assumed in their calculations. This reflects the fact that, in the PTG picture the doped charge is almost exclusively located in the apical $d_{z^2-r^2}$ orbitals of the copper. Therefore, we have drawn a flat dashed line as the PTG prediction for this parameter in Fig. 2(b). As is apparent, the data for $r_{\text{Cu-O}1}$ slope downward with a slope of $\Delta r_{\text{Cu-O}1} \sim -0.105$. This is comparable to, though slightly less than, the observed $\Delta r_{\text{Cu-O}2} \sim -0.18$ of the apical bond. This observation will be important later.

The presence of the anti-Jahn-Teller distorted doped CuO_6 octahedra in the PTG calculations will manifest itself in an increased atomic displacement factor for O2, especially along z . The most sensitive parameter will be the width of the Cu-O pair distribution along the z -axis. This cannot be measured directly from the PDF because of peak overlap but can be found from the sum of $U_{33}(\text{Cu}) + U_{33}(\text{O}2)$. The mean-square width is plotted in Fig. 3 and does increase with increasing doping at constant temperature, a sign that static disorder associated with this bond is increasing with doping. To investigate more quantitatively whether this increase is consistent with the PTG predictions we calculated the PDF of a model structure containing the PTG defects.

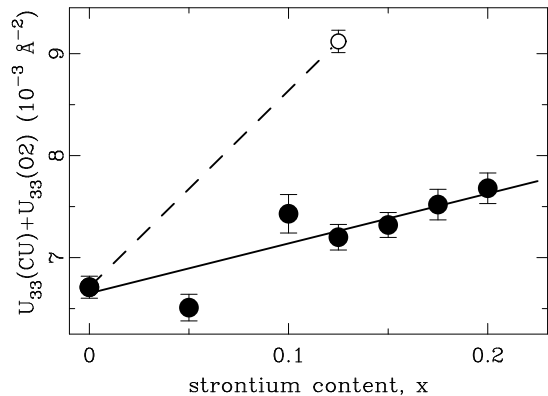


FIG. 3: Sum of displacement parameters U_{33} for Cu and $\text{O}2$ as a function of strontium content at 10 K, from PDF refinements. Solid line is a guide to the eye. Dashed line denotes expected increase in the PDF displacement parameters, estimated from PDF simulation based on PTG model for 1/8 doping (see text).

This simulated PDF was then fit using PDFFIT using the standard LTO model. This gives us a measure of how much $U_{33}(\text{O}2)$ would increase in a standard LTO-structure refinement due to the presence of the PTG defects. The PDF was simulated for the $x = 0.125$ composition using a $8x$ unit cell in the following way. The reference structure used was that of the undoped material with atomic positions taken from³ and displacement factors taken from our PDF result for the undoped sample. One La in the supercell was then replaced with Sr and the atoms on the CuO_6 octahedron adjacent to the Sr were displaced by the Δ -values from the PTG prediction given above. The displacement parameters in the model retained their values in the $x = 0$ compound. This neglects strain due to the defects, and any stripe or checkerboard doping inhomogeneities in the CuO_2 planes, that would tend to increase displacement parameters further. The resulting PDFs were refined with the standard LTO unit cell. This resulted in an enlarged value of $U_{33}(\text{Cu}) + U_{33}(\text{O}2) = 9.1 \times 10^{-3} \text{ \AA}^{-2}$ plotted on Fig. 3, which overestimates the observed displacement factors.

Next, using PDF data of 1/8 doped $\text{La}_{2-x}\text{Sr}_x\text{CuO}_4$ at 10 K, *explicit modeling* of the anti-JT (A-JT) model was performed. The outcome is compared to the results of the modeling of the standard LTO model. The modeling employed the program PDFFIT¹⁰. A large supercell model was generated that incorporates explicit Sr doping, and allows for defining special doping-affected octahedral units, as described above in accord with Ref.¹. Three distinct variants of the explicit A-JT models were attempted. These variants are distinguished as follows: (1) A model with symmetric A-JT distortion on affected octahedral units (apical Cu-O distances restricted to have the same length). (2) A model with asymmetric A-JT distortion (relevant apical distances are allowed to vary

TABLE I: Standard LTO model versus A-JT defect models: PDFFIT modeling results summarizing relevant distances. All lengths are in Å. Rw is the weighted PDFFIT agreement factor.

	LTO	A-JT(1)	A-JT(2)	A-JT(3)
Rw	0.127	0.122	0.131	0.127
r(Cu-O2)	2.4179(24)	2.4095(25)	2.4119(22)	2.406(3)
	-	2.460(19)	2.450(20)	2.49(4)
	-	-	2.469(19)	2.51(3)
r(La-O2)	2.346(3)	2.354(3)	2.354(3)	2.361(4)
	-	2.305(20)	2.305(20)	2.27(4)
r(Sr-O2)	2.346(3)	2.27(3)	2.27(3)	2.20(5)

independently), and (3) A model with asymmetric A-JT distortion this time restricted to have displacements along LTO c -axis only. In all three variants atomic parameters of Sr were decoupled from those of La, except for the displacement factors that were restricted to be the same. In the variant (3) Sr y -coordinate was set to zero and Sr motion was restricted to be along c -axis only. The A-JT models were refined from the same set of initial values as that used for modeling the standard LTO structure. This equality of the starting values was only violated for O2 and Sr fractional y -coordinates in the variant (3), where these were set to zero and fixed.

The results are summarized in Table I, where the weighted PDFFIT agreement factors (Rw)¹⁰ are reported, as well as all relevant distances. Although for all the variants of the A-JT model the agreement factor is similar to the one for the LTO model, and for some variants even somewhat more favorable, it is not sufficient to unambiguously favor the distorted model over the standard LTO structure. Moreover, the refined distortions obtained from such explicit modeling yield relevant distance changes in the direction *opposite* to that originally proposed within the A-JT model of Perry *et al.*¹ (i.e., the Cu-O2 distance of the affected octahedral unit lengthens, while r_{Sr-O2} shortens). However, inspection of the distances for the A-JT model results in the proper weighted average values when compared to corresponding average distances obtained by employment of the standard LTO model.

We now consider the expected structural changes that would occur based on electrostatic considerations in the conventional doping model. First, we note that the charge of the CuO₂ plane is becoming less negative with doping which could result in the apical O²⁻ moving closer to the plane. A very rough estimate of this behavior is possible neglecting the Jahn-Teller effect and assuming an ionic picture by using ionic radii of O²⁻ = 1.35 Å, Cu²⁺ = 0.73 Å, Cu³⁺ = 0.54 Å, La³⁺ = 1.16 Å, and Sr²⁺ = 1.26 Å¹³. From this we get $\Delta r_{Cu-O2} = -0.19 x$ and $\Delta r_{La/Sr-O2} = 0.1 x$ which appear in Fig. 2 as dotted lines. Not surprisingly, these curves are similar to those predicted by PTG that is also a model involving a mix-

ture of Cu²⁺ and Cu³⁺ sites. Uniform doping of charge into the Cu-O planes would not result in an increase in $U_{33}(O2)$ on its own; however, the presence of misfitting Sr²⁺ dopant ions would. Any inhomogeneous charge distribution in the plane would increase $U_{33}(O2)$. The fact that the observed increase in $U_{33}(O2)$ exists but is smaller than needed to explain the PTG defects may argue in favor of electrostatic interpretation. There is a suggestion from single crystal refinements compared with empirical potential calculations that increases in displacement factors with doping can be explained in this way without invoking PTG-type defects¹⁴. Our results would tend to support this.

A more refined empirical framework for studying the distribution of charge between bonds is the bond valence model¹⁵. In this theory there is a direct relationship established between bond-length, r , and the amount of charge in a bond (the bond-valence, s). The bond valence is defined as

$$s(r) = \exp \frac{(r_0 - r)}{B}, \quad (2)$$

where $B = 0.37 \text{ \AA}$ is a universal constant and r_0 depends on the chemical identity of the ions in question. Using this approach it is possible to determine how much of the doped charge is going into the planar vs. the apical bonds from a measurement of their length changes. The theory is successful in unstrained compounds and has recently been applied to mixed valent crystals and crystals containing Jahn-Teller distortions¹⁶. The nominal valence, V_i , of an ion is then determined by summing the bond-valences over all the bonds in which it participates, $V_i = \sum_j s_{ij}$. In the case of mixed valent crystals some ambiguity exists as to exactly what value to use for r_0 . The qualitative results of our analysis, however, do not depend on what value of r_0 is used. The results are shown in Fig. 4. Here we plot how the total doped charge (assumed to be given by x) distributes itself between the apical and planar orbitals respectively, as determined from the bond-valence sums. The dimensionless variables, η_p (solid circles) and η_a parameterize this partition where $\eta_p + \eta_a = 1$.

Details of these calculations are as follows. First we determine the change in bond-valence of a particular bond due to doping, $\delta s_i(x) = s_i(x) - s_i(0)$. We are interested in the partition of charge between the planar and apical orbitals, therefore we define an orbital-valence $\delta S_m = \sum_i \delta s_i$ where the sum is over the planar bonds for the $Cu d_{x^2-y^2} - O p_{x,y}$ orbital, δS_p , and over the apical bonds for the $Cu d_{3z^2-r^2} - O p_z$ orbital, δS_a . This is then expressed in dimensionless parameters by dividing by the total *excess* valence of copper determined by the sum over all the orbital-valences, $\eta_m(x) = \delta S_m(x)/V_{Cu}^{ex}$. What is plotted in Figure 4 is $x\eta_p$ (solid circles) and $x\eta_a$ (solid squares), that are measures of the amount of charge doped into the planar and apical orbitals, respectively.

As is apparent in Fig. 2, *both* the apical and in-plane bonds shorten with doping indicating a reduction in

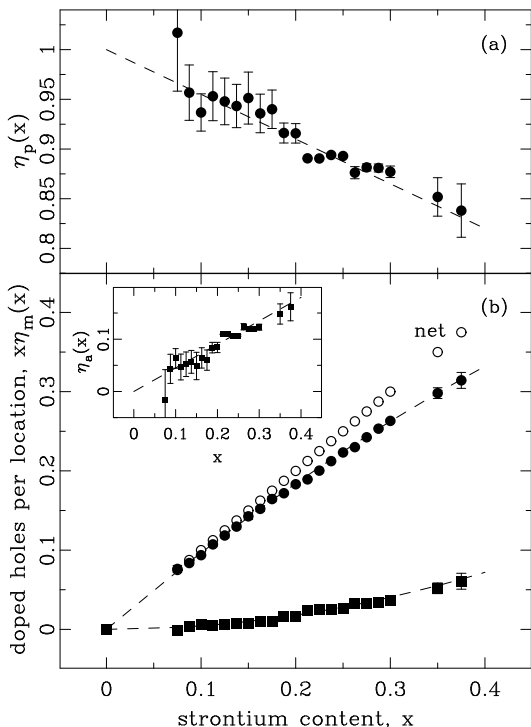


FIG. 4: (a) Partitioning parameter vs. Sr content. (b) Estimated average distribution of doped charge at 10 K based on bond valence calculations using Rietveld obtained distances: net apical share (solid squares), net planar share (solid circles), total doped charge (open circles). Inset: a measure of the amount of charge doped into the apical orbitals. Dashed lines represent fit to the data (see text for details).

charge and doped holes going into both planar and apical bonds. However, one of the key aspects of this theory is the non-linear form of the bond valence, $s(r)$. As a result, the same amount of charge doped into a long-bond shortens it much more than it would a short-bond, and vice versa. At $x = 0$ $r_{Cu-O1} < r_{Cu-O2}$ reflecting the fact that initially the holes that make Cu in the $2+$ -state reside predominantly in the planar orbitals making these the canonical half-filled anti-bonding bands, with the apical bonds being doubly occupied with electrons (i.e., full, no holes). The physics of this is the existence of the Jahn-Teller distortion; however, this shows that the phenomenological bond-valence model is making the correct prediction for the charge segregation initially. Subsequently, the experimental observation is that *both the planar and apical bonds shorten at about the same rate* but because the planar bonds are initially shorter, and the fact that there are four of them rather than two, mean that the experimental observations demand that the doped charge is going predominantly into the planar orbitals as is evident in Fig. 4.

The main result of this analysis is that the simple picture of localized $Cu_{3z^2-r^2}-Op_z$ doped holes associated with Sr sites described by the PTG calculations

is not supported by the structural data. To a rather good approximation doped charge is going into the planar $Cu_{x^2-y^2}-Op_{x,y}$ orbitals. We do not address here whether Cu sites contain different amounts of charge and this does not rule out localized doped defects or striped or checkerboard patterns of charge if they have sufficient planar character. Such defects have been stabilized in the unrestricted Becke-3-Lee-Yang-Parr density functional calculations¹⁷. However, the observation that r_{Cu-O2} is getting shorter also requires that some doped charge is appearing in the apical $Cu_{3z^2-r^2}-Op_z$ orbital and a correction should be made to the canonical $p = x$ relationship to account for this, where p is the doped charge in the planar orbitals. The partitioning parameter η_p gives the correction, and p is therefore given by $p = x\eta_p$ (η_p shown in Fig. 4(a)). This augments spectroscopic measurements that show the partition of charge between copper and oxygen but struggle to differentiate partition between planar and apical bonds^{18,19,20}.

In Figure 4(a) we show η_p on an expanded scale. To obtain an analytic form for the $p(x)$ calibration curve we have fit curves to the data in Fig. 4(a). Linear fit proved adequate resulting in $\eta_p = -0.45(7)x + 1.00(1)$. This results in the calibration

$$p(x) = x(1.00(1) - 0.45(7)x). \quad (3)$$

The resulting fit to the data is shown in Fig. 4(a) and (b) and in the inset as a dashed line. Thus, at a strontium content of $x = 0.125$ the doping in the planar orbitals is actually $p = 0.119$, and conversely, the rational $1/8$ filling occurs at $x = 0.131$. Interestingly, the plateau in resistivity that was observed by Komiya *et al.*¹¹ and correlated with special behavior at $1/8$ doping occurred at $x = 0.13$, which would correspond to $p = 0.125$ when corrected using our calibration curve. Note that, at all dopings, more than 85% of doped charge goes into the planar orbitals, though it appears increasingly in the apical bonds at higher doping.

IV. CONCLUSIONS

In summary, we have tested the hypothesis that doping in $La_{2-x}Sr_xCuO_4$ is occurring predominantly in $Cu_{3z^2-r^2}-Op_z$ orbitals¹, rather than the canonical picture of doping into the planar $Cu_{x^2-y^2}-Op_{x,y}$ bands. Whilst the average structure evolves *qualitatively* as would be predicted according to $Cu_{3z^2-r^2}-Op_z$ doping picture, more quantitative analysis suggests that the canonical picture of one hole doped into the planar bands per strontium is actually rather close to the true situation. We present a correction factor quantifying the partition of doped charge between planar and apical bonds.

Acknowledgments

We would like to acknowledge M. J. Gutmann, A. Bianconi, N. L. Saini and P. G. Radaelli for help and discussions. We acknowledge beamtime on the instru-

ment GEM at ISIS. This work was supported by NSF through grant DMR-0304391. SJB acknowledges support and hospitality from Università di Roma, “La Sapienza”, where part of the work was carried out.

-
- * Electronic address: bozin@pa.msu.edu;
URL: <http://nirt.pa.msu.edu/>
- ¹ J. K. Perry, J. Tahir-Kheli, and W. A. Goddard-III, *Phys. Rev. B* **65**, 144501 (2002).
 - ² D. Haskel, E. A. Stern, D. G. Hinks, A. W. Mitchell, and J. D. Jorgensen, *Phys. Rev. B* **56**, R521 (1997).
 - ³ P. G. Radaelli, D. G. Hinks, A. W. Mitchell, B. A. Hunter, J. L. Wagner, B. Dabrowski, K. G. Vandervoort, H. K. Viswanathan, and J. D. Jorgensen, *Phys. Rev. B* **49**, 4163 (1994).
 - ⁴ S. J. L. Billinge and M. G. Kanatzidis *Chem. Commun.* 749 (2004).
 - ⁵ E. S. Božin, S. J. L. Billinge, G. H. Kwei, and H. Takagi, *Phys. Rev. B* **59**, 4445 (1999).
 - ⁶ E. S. Božin, Ph.D. thesis, Michigan State University, 2003.
 - ⁷ A.C. Larson and R.B. Von Dreele, Los Alamos Nat. Lab. Rep. LAUR 86-748 (1994).
 - ⁸ T. Egami and S. J. L. Billinge, *Underneath the Bragg Peaks: Structural analysis of complex materials*, Pergamon Press, Elsevier, Oxford, England, 2003.
 - ⁹ P. F. Peterson, M. Gutmann, Th. Proffen, and S. J. L. Billinge, *J. Appl. Crystallogr.* **33**, 1192 (2000).
 - ¹⁰ Th. Proffen and S. J. L. Billinge, *J. Appl. Crystallogr.* **32**, 572 (1999).
 - ¹¹ S. Komiya, H.-D. Chen, S.-C. Zhang, and Y. Ando, *Phys. Rev. Lett.* **94**, 207004 (2005).
 - ¹² T. Hanaguri, C. Lupien, Y. Kohsaka, D.-H. Lee, M. Azuma, M. Takano, H. Takagi, and J. C. Davis, *Nature* **430**, 1001 (2004).
 - ¹³ R. D. Shannon and C. T. Prewitt, *Acta Cryst. B* **25**, 925 (1969).
 - ¹⁴ M. Braden, M. Meven, W. Reichardt, L. Pintschovius, M. T. Fernandez-Diaz, G. Heger, F. Nakamura, and T. Fujita, *Phys. Rev. B* **63**, 140510 (2001).
 - ¹⁵ I. D. Brown and D. Altermatt, *Acta Cryst. B* 41 (1985) 244.
 - ¹⁶ I. D. Brown, *J. Solid State Chem.* **82**, 122 (1989).
 - ¹⁷ J. Tahir-Kheli, (private communication).
 - ¹⁸ C. T. Chen, F. Sette, Y. Ma, M. S. Hybertsen, E. B. Stechel, W. M. C. Foulkes, M. Schluter, S-W. Cheong, A. S. Cooper, L. W. Rupp, Jr., B. Batlogg, Y. L. Soo, Z. H. Ming, A. Krol, and Y. H. Kao, *Phys. Rev. Lett.* **66**, 104 (1991).
 - ¹⁹ C. T. Chen, L. H. Tjeng, J. Kwo, H. L. Kao, P. Rudolf, F. Sette, and R. M. Fleming, *Phys. Rev. Lett.* **68**, 2543 (1992).
 - ²⁰ B. Dalela, S. Dalela, N. L. Saini, R. K. Singhal, C. T. Chen, and K. B. Garg, *Int. J. Mod. Phys. B* **18**, 2849 (2004).